Synthesis and Characterization of Polysulfone/Clay Nanocomposite Membranes for Fuel Cell Application

Lakshmi Unnikrishnan, Smita Mohanty, Sanjay K. Nayak, Nishant Singh

Laboratory for Advanced Research in Polymeric Materials (LARPM), Central Institute of Plastics Engineering and Technology, Bhubaneswar 751 024, India

Received 18 August 2009; accepted 16 February 2011
DOI 10.1002/app.34355
Published online 2 February 2012 in Wiley Online Library (wileyonlinelibrary.com).

ABSTRACT: In the present investigation, polysulfone (PSu) nanocomposites were successfully prepared by solvent casting method. Layered silicates, viz., sodium montmorillonite (NaMMT), Cloisite 93A, and Cloisite 30B were dispersed in PSu to obtain nanocomposite membranes. PSu nanocomposite membranes were tested for mechanical performance, water uptake, thermal properties, X-ray diffraction, and scanning electron microscopy (SEM). The nanocomposite membranes showed an increment in tensile properties, whereas a reduction was observed in water uptake. X-ray diffraction studies confirmed the intercalation of PSu within the silicate galleries. SEM analysis confirmed an increase in the porosity of the membrane with the incorporation of nanoclays. Thermo gravimetric analysis (TGA) thermograms indicated an increase in the thermal stability of PSu nanocomposites. Evaluation of conductivity characteristics and single cell performance revealed improved output for organomodified clay nanocomposites. © 2012 Wiley Periodicals, Inc. J Appl Polym Sci 124: E309–E318, 2012

Key words: polysulfone; impedance spectroscopy; scanning electron microscopy; nanoclays; proton conductivity

INTRODUCTION

Pollution control has stimulated the development of polymer electrolyte membrane fuel cells (PEMFCs), which have attracted increasing attention, particularly for automotive and stationary power applications.[1–3] For all applications, including generation of electricity, PEMFCs prove to be the most promising fuel cell due to their modularity. Nafion dominates the market of ionomeric membranes for fuel cell, satisfies the requirements of high proton conductivity below 100°C and high chemical stability. The high cost and very high methanol permeability limit its application in direct methanol fuel cells. Fuel cell operated at temperatures up to 150°C, have improved reaction kinetics, thus reducing the catalyst poisoning by carbon monoxide (CO). However, in the case of Nafion membranes, rapid dehydration above 100°C leads to a drastic reduction in its properties.[4] Trifluorostyrene membranes (BAM3G), developed by Steck et al.,[5] have also demonstrated good performance characteristics along with long-term stability. To overcome the disadvantages of perfluorinated ionomers membranes, several efforts were made to substitute them with a viable alternative. High-performance engineering plastics, such as polyketones[6–9] and polysulfones (PSus),[10–12] have proved to be a suitable laternative because of their high chemical and thermal stability.[13,14] Among various engineering plastics, PSu is the preferred material for fuel cell applications owing to its low cost and easy availability.[12,15] High redox stability in wide temperature range, high glass transition temperature, and solubility in organic solvents used for modifications and high thermal stability account for its candidature.[16] Moreover, PSu is completely amorphous, and therefore, its mechanical strength does not depend on crystallinity ration or melting temperatures.

Introduction of fillers in the nanoscale level leads to an increase in the overall properties of the virgin polymer. Recently, interesting applications of nanocomposite membranes have been reported in the field of fuel cells. Alberti et al.[17] reported the use of layered zirconium sulfoarylphosphonates to prepare composite membranes with high proton conductivity and good stability at medium temperatures. Organic and inorganic nanoclays are being used as fillers in polymer matrix for manufacturing nanocomposite membranes that can be used as electrolyte for PEM fuel cell. When polymers are mixed with these inorganic materials, there is an increase in mechanical strength and a considerable decrease in the permeability of gases such as oxygen and moisture.[18] Nafion/montmorillonite (MMT) nanocomposite membranes have been identified as an efficient candidates for direct methanol fuel cells.[19] Some of the new reports

Correspondence to: S. K. Nayak (papers.journal@gmail.com).

include the use of heteropolyacids in sulfonated polyether ether ketone (SPEEK)[8] and SPSU[20] and phosphate in PEEK[21] for this purpose. Among the various inorganic fillers, zeolites have been studied with rubbery polymer matrix like EPDM[22] as well as PDMS.[23] On the other hand, the layered silicates have been chosen from ceramic oxides family to prepare composite membranes and films, layered silicates deserve a special attention because of their ability to disperse within the polymeric matrices like polyvinylidene fluoride (PVdF), polyimide, PSu, and Poly(4-methyl 2-pentyne)[24–27] at a nanoscopic level. It has also been that proton conduction occurs through the ionic channels formed by micro- or nanophase separation between the hydrophilic proton exchange sites and the hydrophobic domains.[28,29] The nanocomposites consisting of exfoliated-layered silicates[30,31] exhibit superior physical and mechanical properties, including enhanced Young's moduli,[32–36] reduced gas permeability,[37–40] and increased heat and flame resistance.[41,42] MMT has been used to improve the performances of Nafion®[43] and SPEEK fuel cell membranes[44] with a special effort for decreasing the methanol permeability and preventing excessive swelling at high temperature.

However, the addition of multi-layered aluminosilicates results in decreased ionic conductivity because the dispersed clay particles prohibit polymer movement.[45] The proton-conducting characteristics depend on the size and distribution of the pores as well as the nature of the filler. The conductivity depends on the particle–particle paths connecting the external faces of the membrane and suitable segregation of inorganic fillers inside the polymeric matrix favoring the formation of these paths. The layered silicate particles are formed parallel to the pore surface, and this orientation increases the proton conductivity in the direction perpendicular to the membrane. An increased length of the transport pathway may result in reduced proton conductivity.[46]

The conductivity also depends on the dispersion of nanoclays within the polymer matrix. Exfoliated-layered silicates act as a reasonable barrier for methanol permeation along with either enhancing or least not interfering with proton conduction. With an increase in clay loading, the room temperature proton conductivity decreased.[47] It was observed that the intercalated structures are more efficient in decreasing methanol permeability. However, modification of nanoclays to replace Na^+ ions with H^+ ions shall further increase the proton mobility through composite membranes.[44]

In this communication, we report the performance characteristics of PSu/layered silicate nanocomposite membranes, fabricated through solvent casting method. The effect of nanofillers on the conductivity and fuel cell performance has been studied. Unmodified as well as modified nanoclays were dispersed in the PSu matrix. The membranes were characterized for mechanical properties, water uptake, and thermal behavior [differential scanning calorimetry (DSC) and thermogravimetric analysis]. The polymer intercalation within the silicate layers was examined from X-ray diffraction pattern. Further, the scanning electron micrograph revealed the surface morphology of the membranes.

EXPERIMENTAL

Materials

PSu (MFI = 6.50 g/10 min, M_n = 16,000 and M_w = 35,000) was purchased from M/s Sigma Aldrich, Germany. *N*,*N*-dimethyl formamide (DMF) having boiling point = 153°C and density = 0.944 g/cm^3, obtained from M/s S D FINE Chem., Mumbai, was used as the solvent. Organoclays, viz. sodium montmorillonite (NaMMT), Cloisite 30B (C30B), and Cloisite 93A (C93A) were obtained from M/s Southern Clay Products, Gonzales. C93A was modified by methyl dehydrogenated tallow ammonium salt, whereas C30B contained a methyl tallow bis-2-hydroxyethyl quaternary ammonium salt as surfactant. Commercially available Nafion membrane was purchased from M/s Ion Power Inc., New Castle for comparative study of fuel cell performance.

Preparation of membranes

PSu was dissolved in 20 mL DMF at 45°C with continuous stirring to obtain 15 wt % solution. NaMMT, C93A, and C30B nanoclays were added to the prepared solution in desired amount to prepare a ternary dispersion. The solution was stirred continuously for 12 h to properly disperse the clay platelets. Subsequently, solution was cast onto a glass plate and exposed to a controlled environment [23°C ± 2°C and 50% ± 5% relative humidity (RH)] for 1 min. The membranes were prepared by evaporating the solvent (DMF) from the cast solution by exposing in an air circulating oven at 90°C for 12 h.

Tensile properties

Specimens of dimension 20 mm × 100 mm were prepared from cast membranes of 50 μm thickness for determining tensile strength, tensile modulus, and elongation at break as per ASTM D 882. The test was carried out in Universal Testing Machine (LR 100K, M/s Lloyds Instruments, UK) with an operating head load of 1 kN. The gauge length was fixed at 50 mm, and the tests were carried out at a cross-head speed of 12.5 mm/min. Five replicate specimens were taken for each test, and the average of five samples as well as corresponding standard deviation is reported.

Water uptake

The water absorption in the samples was measured by immersing the membranes in water at room temperature for a period of 1 week. The weight of dry membranes was recorded as "W_d." The weight of the wet membrane, "W_w," was recorded periodically after 24 h, 48 h, and 1 week. Excess water was removed from the surface of the membrane, and the final wet weight, W_w, was measured.

Percentage water absorption was calculated using the following formula:

$$\text{Water uptake } (\%) = (W_w - W_d) \times 100/W_d$$

Morphological studies

Scanning electron microscopy

The surface morphology of virgin PSu and PSu/clay nanocomposite membranes was studied using scanning electron microscopy (SEM) HITACHI *S*-3400*N*, Japan. The pore distribution as well as clay dispersion in the membranes were analyzed. The samples were conditioned for 1 h and sputter coated with gold prior to testing.

The porosity of the membranes has also been studied using SEM. After 1–2 min of gentle rinsing in distilled water, the membrane was removed and placed on the Peltier cooling device inside the SEM chamber. The samples were kept wet by using the Peltier cooling device maintained at 4°C and a chamber water vapor pressure between 4.5 and 5.5 Torr. Water vapor was allowed to condense on the cooled target to keep it moist, while the imaging was performed. The average pore size was calculated in the virgin PSu and all the nanocomposite membranes.

2.5.2 Wide angle X-ray diffraction

X-ray diffraction patterns of membranes were collected using Philips X'Pert MPD, Japan, with Cu Kα radiation source. These patterns were used to determine the interlayer spacing (gallery distance) of the (001) plane (d_{001}) for organoclays C30B, C93A, and PSu/C30B, PSu/C93A nanocomposites. The experiments were carried out in the 2θ range of 1–10° at a scanning rate of 2°/min and a voltage of 40 kV.

Thermal properties

Thermo gravimetric analysis

Thermal degradation behavior of the PSu nanocomposite membranes was investigated using a thermogravimetric analyzer (Pyris 7 TGA, M/s Perkin Elmer, California) within a temperature range of 50–700°C, at a heating rate of 10°C/min under nitrogen atmosphere. The degradation temperature and ash content were recorded using 5–10 mg samples, wherein percentage weight loss was determined as a function of temperature.

Differential scanning calorimetry

Virgin PSu as well as nanocomposite films were analyzed by DSC using Diamond DSC (M/s Perkin Elmer, California). The characteristic thermal properties such as glass transition and melting point were determined using DSC. Temperature calibration was performed using Indium as a reference (T_m = 156.60°C and Heat flow = 28.5 J/g). The test was conducted within a temperature range of 50–300°C at a heating rate was 5°C/min under nitrogen atmosphere. The baseline was calibrated using empty aluminum pans. Samples with mass of 5–10 mg were used for all DSC experiments.

Proton conductivity

The ionic conductivity of PSu nanocomposites was determined from impedance spectra obtained from the Gill AC Impedance Spectroscope (M/s ACM Instruments, Cumbria). The conductivity was analyzed within a frequency range of 30–30,000 Hz at variable temperatures from 30 to 60°C and 100% RH. The samples, 1.13 cm^2 in area, were placed between the electrodes to determine the resistivity of the membrane for further calculation of conductivity. Average conductivity of three samples has been reported.

Fuel cell performance

The virgin PSu, PSu/clay nanocomposite membranes, and commercial Nafion membranes were hot-pressed between standard electrodes with Pt loading (0.5 mg cm^{-2}) for anodes and cathodes in the catalyst layer, with a low-PTFE content in the diffusion layer. The fuel cell performance was characterized by current–voltage measurements (polarization curves) that were recorded at 70 and 110°C and atmospheric pressure. The obtained membrane electrode assemblies (MEAs) were characterized in a 5 cm^2 commercial single cell. The gas fluxes were fixed at 1.5 times the stoichiometry for the fuel and twice the stoichiometric value for the oxidant at a current density of 1.0 Acm^{-2}. MEAs were tested in the temperature range 70–110°C in H_2/air, maintaining the gas humidifying temperature 10°C at the anode and 5°C at the cathode higher than the cell temperature at 3.0/3.0 abs bar. The polarization curves were recorded by means of a test station equipped with software for automatic data

TABLE I
Tensile Properties of PSU and its Nanocomposite Membranes

Sample	Tensile strength (MPa)	Tensile modulus (MPa)	Strain at break (%)
PSu	25.14 ± 0.10	1142.56 ± 36.87	5.76 ± 0.24
PSu/0.5 % C30B	11.65 ± 0.85	1322.8 ± 55.87	1.48 ± 0.15
PSu/1% C30B	22.08 ± 1.56	2899.73 ± 42.23	3.16 ± 0.22
PSu/2% C30B	9.45 ± 0.98	1613.6 ± 50.74	1.80 ± 0.03
PSu/0.5% C93A	10.99 ± 1.42	1524.44 ± 44.23	1.16 ± 0.04
PSu/1% C93A	19.58 ± 1.31	2179.13 ± 59.40	3.40 ± 0.40
PSu/2% C93A	17.25 ± 0.98	2044.28 ± 49.77	2.12 ± 0.23

acquisition, and the cell resistance was measured with an Agilent milli ohmmeter by a static method at a frequency of 1 kHz.

RESULTS AND DISCUSSION

Mechanical properties

The mechanical properties of virgin PSu and PSu-clay nanocomposite membranes are represented in Table I. It is observed that virgin PSu has a tensile modulus of 1142.56 MPa. With the incorporation of nanoclay to the tune of 0.5–1%, there was a significant increase in the modulus, which is probably due to the inherent high aspect ratio of nanoscale platelets, which exhibits a synergistic effect when dispersed at a nanoscale level, thus enhancing the moduli in the nanocomposite.[48]

Addition of 1 wt % C30B resulted in an increase in the modulus to the tune of 150% to 2899 MPa as compared with virgin PSu. This confirms the reinforcing effect of the nanoscale particles resulting in effective stress transfer at the interface. Also it is assumed that the hydrogen bonding between matrix polymer and hydroxyl groups present in the intercalant in C30B might have led to the increase in tensile modulus. A similar increase in tensile modulus to 100% increase to 2179 MPa was noticed with the incorporation 1 wt % C93A. This phenomenon is probably due to the interaction between tallow group of C93A and PSu.

However, with the increase in the clay concentration to 2 wt %, there was a marginal decrease in modulus in all the cases. PSu/2 wt % C30B nanocomposite showed a modulus of 1613 MPa which was reduced by 44% as compared with the nanocomposite film prepared using 1 wt % C30B. This decrease in modulus is primarily attributed to agglomeration of silicate layers on the film surface due to improper dispersion. PSu/C93A nanocomposites also showed a decrease in modulus to the tune of 6% to 2044 MPa with 2 wt % clay loading. Comparing the test results, it could be concluded that PSu/C30B exhibited optimum properties, which may be probably due to the effective interaction between the polar groups of the matrix polymer and hydroxyl groups in intercalant present in C30B. However, the high hydrophobicity due to the presence of two hydrogenated tallow along with one methyl group in the surfactant of C93A imparts lesser interaction with PSu matrix as compared with C30B.

As evident from the test results reported in Table I, virgin PSu showed a tensile strength of 25.14 MPa, which decreased with the addition of organo-modified clay. Incorporation of 1 wt % C30B showed a tensile strength of 22.08 MPa with 12% decrement in comparison to virgin PSu. Tensile strength reduced to the tune of 62% as compared with virgin PSu in presence of 2 wt % C30B. The addition of clay has rendered the polymer brittle resulting in the decrease of tensile strength. The increase in crystallinity with the addition of nanoclays has probably contributed to the significant decrease in tensile strength. In the case of PSu/1 wt % C93A nanocomposite film, tensile strength of PSu matrix reduced from 25.14 to 19.57 MPa. This phenomenon is probably due to lack of proper dispersion of C93A in PSu and less favorable interaction between the clay and PSu matrix.

Virgin PSu exhibited optimum elongation of 1.45 mm, which decreased significantly in the nanocomposite films, primarily attributed to the presence of rigid-layered silicate modifier. Elongation at break of the matrix polymer also reduced in all the cases with the incorporation of nanoclays. Incorporation of 1 wt % C30B resulted in a decrease in elongation by 45%, wherein the rigid inorganic filler imparted brittleness of the films obtained. A marginal decrease to the tune of 41% in elongation was observed for PSu/1 wt % C93A nanocomposite as compared with virgin PSu films. At a higher filler loading of 2 wt %, the elongation was further reduced to 63% in PSu/C30B nanocomposites, which may be attributed to the presence of rigid fillers.

Due to high brittleness characteristics of PSu/NaMMT nanocomposite films, which may be attributed to the incompatibility of the polar clay with the polymer as reported in various other nanocomposite systems,[48] the mechanical properties could not be measured. The optimized samples were subjected to further characterization studies.

Water uptake

The water uptake capacity of polymers has profound effect on proton conductivity. Higher water uptake

generates a more solvated species, which is necessary for high conductivity, whereas enhanced water content produces mechanically less stable membranes. The proton-conducting polymers generally possess phase separated morphology with hydrophobic and hydrophilic phases of which the hydrophilic domain forms a continuous pathway for conduction. The polymeric phase stabilizes the morphology of the membrane by balancing the swelling pressure of water against mechanical strength. The water uptake for all the samples was measured and depicted in Table II. Virgin PSu membrane exhibited higher water uptake in comparison to the nanocomposite membranes. Virgin PSu showed a water uptake of 169% after 24 h at room temperature. The water uptake was increased to 194% after 48 h which remained constant thereafter thus indicating saturation level. This higher water uptake in the matrix polymer is probably due to inherent polarity of PSu matrix. Moreover, the membrane morphology was found to be highly porous, which would have contributed to the cited results. Large water domains result in lower water–polymer interaction thus leading to decreased conduction properties.

The water uptake of the nanocomposite membranes decreased with the incorporation of nanoclay, because inorganic nanoparticles reduce the membrane free volume and swelling ability as explained by Prasantha and Park.[49] The silicate layers provide continuity of hydrophilic phases, which is important for ion transport of the conducting membranes. PSu/1 wt % NaMMT nanocomposite membrane exhibited saturation after 24 h with a water uptake of 31%.

PSu/1 wt % C30B nanocomposites showed water uptake of 34%, 36%, and 39% after 24 h, 48 h, and 1 week of immersion, respectively. There was no appreciable change in water uptake with time at room temperature. The proton-conducting polymer phase separate on hydration thus forming a percolating network of nanometric pores, which results in the formation of hydrophilic domain embedded within hydrophobic phase and generates a continuous pathway for proton conduction. Also as evident from the SEM micrographs (discussed in later section) of PSu/1 wt % C30B, the pore size as well as density were increased with incorporation of inorganic fillers thus providing sufficient channels for proton conduction. PSu/1 wt % C93A nanocomposites showed a water uptake of 28% after 24 h of immersion, which increased to 45% after 48 h. Subsequently, the membranes attained a saturation level.

The water uptake was increased with the incorporation of 2 wt % nanoclay as compared with 1 wt % nanocomposite membrane in all the cases. This may be due to the agglomeration of silicate layers and increased porosity of the membranes reinforced with higher concentration of nanoclays. At higher clay loading, PSu/2 wt % NaMMT nanocomposites showed the highest water uptake similar to that of virgin PSu, which may be attributed to the hydrophilic nature of the filler. Thus, from the test results, it could be noticed that PSu/C30B nanocomposites exhibited optimum water uptake with a nominal value that is sufficient for effective proton conduction.

TABLE II
Water Uptake of Nanocomposite Membranes

Samples	Water uptake (%)		
	24 h	48 h	1 week
Virgin PSu	169 ± 0.85	194 ± 0.89	194 ± 0.90
PSu/1% NaMMT	31 ± 0.96	31 ± 0.92	31 ± 0.94
PSu/2% NaMMT	128.6 ± 0.93	153 ± 0.86	187 ± 0.78
PSu/1% C30B	34 ± 0.77	36.8 ± 0.81	39.7 ± 0.86
PSu/2% C30B	55.3 ± 0.91	56.3 ± 0.88	59.7 ± 0.89
PSu/1% C93A	28.43 ± 0.89	45 ± 0.90	45 ± 0.87
PSu/2% C93A	26 ± 0.98	26 ± 0.96	31 ± 0.91

Morphological studies

Scanning electron microscopy

The surface morphology of virgin PSu and PSu/NaMMT, PSu/C30B and PSu/C93A nanocomposites were studied using SEM as displayed in Figure 1. The micrograph of virgin PSu revealed the distribution of small pores on the surface of the membrane. These pores may be considered as the hydrophilic channel for proton conduction. The removal of solvent during evaporation has led to the formation of pores on the surface. Similar phenomenon was observed by Smitha et al.[4] for PSu-heteropolyacid composite membrane. Unlike virgin PSu, nanocomposite membranes exhibited larger, but less number of pores on the surface. This might have led to the decrease in water uptake of the nanocomposite membranes, as explained in the former section. This phenomenon can be attributed to the quick exchange between the solvent phase and nonsolvent phase leading to immediate phase inversion. Similar behavior has also been studied by Luo et al.[50] for polyether sulfone-TiO_2 composite membrane.

The number of pores and pore size could affect the proton conduction, because they are the channels through which protons move rapidly. The average pore size of PSu/NaMMT nanocomposites was found to be 18.27 μm, which increased to 24.97 μm in PSu/C93A, limiting its use as a polymer electrolyte membrane. Further, these membranes exhibited distorted structure with improper distribution of pores. The pore size distribution was found to be satisfactory in the case of PSu/1 wt % C30B nanocomposite, which displayed an average pore size of 0.857 μm. This confirms effective proton conduction through the nanometric pores in PSu nanocomposites with organically modified C30B clay. The pores also help in retaining water, which act as a gelation

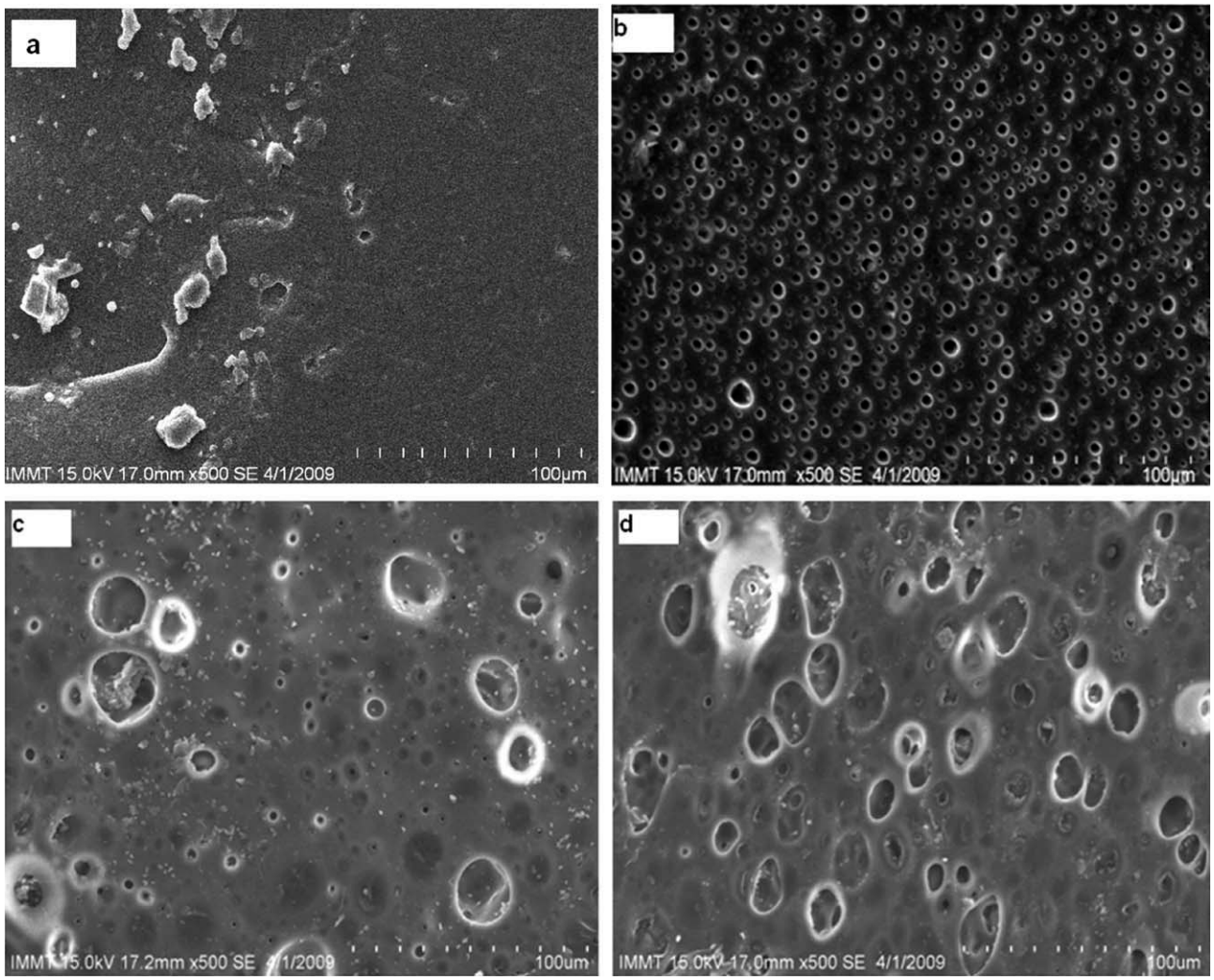

Figure 1 SEM micrographs of (a) Virgin PSu, (b) PSu + 1% C30B, (c) PSu + 1% C93A, and (d) PSu + 1% NaMMT.

medium to enable efficient proton conduction. Conversely, incorporation of NaMMT in PSu matrix yielded a completely deformed surface that may result in reduced conduction characteristics. The PSu/C30B nanocomposite membranes were observed to have better pore distribution characteristics and are therefore proposed to exhibit stable conductivity.

Wide angle X-ray diffraction

To confirm polymer intercalation into the organomodified silicate layer, the increase in *d*-spacing was measured by X-ray diffraction technique. It is evident from Figure 2 that C30B showed a diffraction peak corresponding to $2\theta = 5.8^\circ$ and the *d*-spacing, as calculated by Bragg's equation $n\lambda = 2d \sin\theta$, where $n = 1$, was found to be 18.5Å. Similarly, C93A showed a diffraction peak at $2\theta = 3.62^\circ$ with *d*-spacing of 24.4Å. The wide angle X-ray diffraction (WAXD) pattern of PSu/1 wt % C30B nanocomposite reveals a diffraction peak at $2\theta = 2.63^\circ$ corresponding to a *d*-spacing of 24.3Å. The shift of diffraction peak towards lower angle is the signature of chain intercalation, wherein the PSu chains have entered into the clay galleries of C30B forcing the clay platelets apart, thus increasing the *d*-spacing from 18.5Å in pristine clay to 24.3Å in the nanocomposite. This behavior is probably due to interaction between hydroxyl groups of C30B and matrix polymer.[48]

In the case of PSu/1 wt % C93A nanocomposite, there was no appreciable change in the diffraction peak indicating irrelevant intercalation of PSu chains within C93A clay galleries. The peaks at $2\theta = 6.54^\circ$ and 7.48° for C93A and C30B, respectively, indicates clay agglomeration which can be attributed to the improper clay dispersion within the base polymer.[48]

Thermal properties

Thermo gravimetric analysis

The degradation behavior of virgin PSu and nanocomposite membranes is shown in Figure 3. The thermogram displayed single-step degradation for virgin as well as nanocomposite membranes.

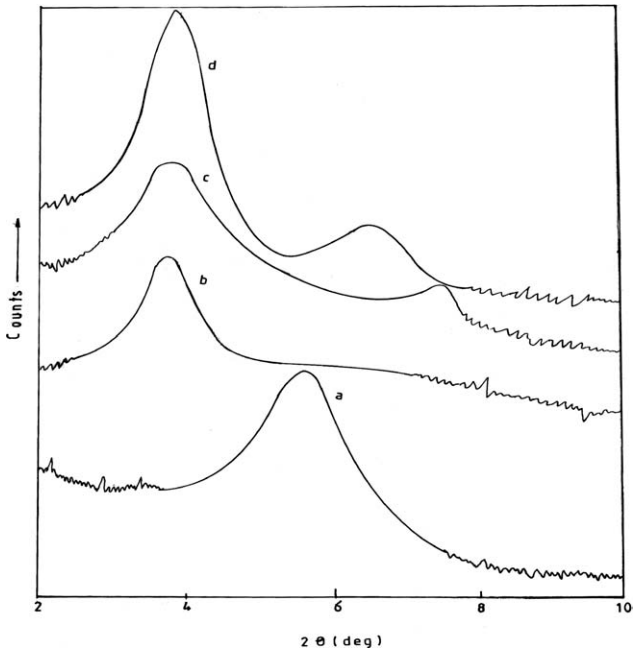

Figure 2 XRD patterns of (a) C30B, (b) C93A, (c) PSu + 1% C30B, and (d) PSu + 1% C93A.

Incorporation of 1 wt % NaMMT resulted in marginal increase in initial degradation temperature (T_i) to 523°C from 515°C for virgin PSu. Incorporation of organically modified clays C30B and C93A also exhibited an increase in T_i to 525 and 530°C in PSu/1 wt % C30B and PSu/1 wt % C93A nanocomposites, respectively. The inherently thermostable clay layers dispersed within the matrix led to the increase in T_i.

The improvement in thermal stability may be attributed to the intercalation of polymer matrix into the clay galleries, which act as a barrier for thermal degradation of the polymer. PSu/C30B nanocomposite showed comparatively lesser thermal stability as compared with PSu/C93A nanocomposites, which is probably due to the presence of hydroxyl groups in the C30B nanoclay. Similar results for PS/clay nanocomposite membranes investigated by Jang and Walkie[51] substantiates our experimental findings.

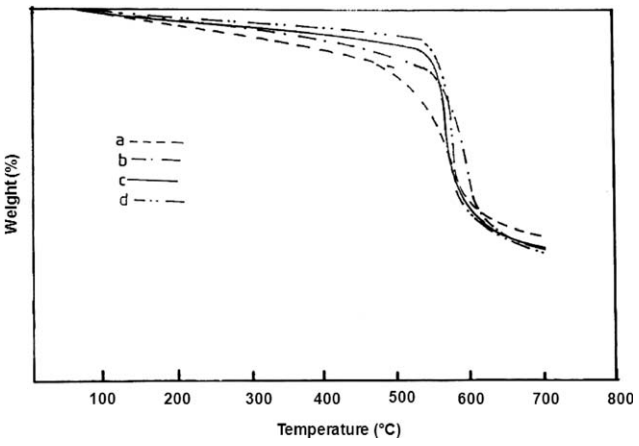

Figure 3 Thermal properties of (a) virgin PSu, (b) PSu + 1% NaMMT, (c) PSu + 1% C93A, and (d) PSu + 1% C30B.

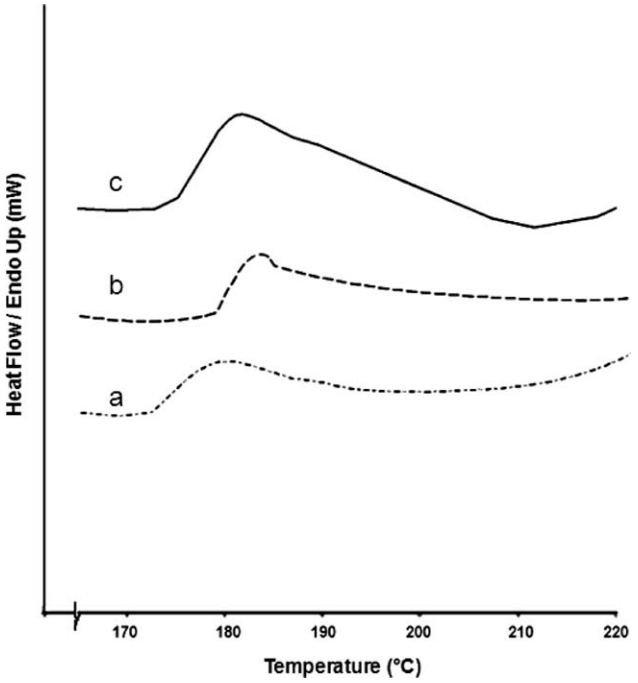

Figure 4 DSC thermograms of (a) virgin PSu, (b) PSu + 1% C30B, and (c) PSu + 1% C93A.

Moreover, the high-performance polymer PSu employed in the study was not completely degraded within the test temperature leaving behind 35% residue at 700°C. This reveals the superior thermal stability of PSu thus ensuring optimum performance in high temperature fuel cells applications.

Differential scanning calorimetry

The DSC thermograms of virgin PSu and its nanocomposites are represented in Figure 4. Only the glass transition could be detected within the test temperature range. The thermogram shows that virgin PSu has a T_g around 177°C. It is observed that with the incorporation of 1 wt % C30B nanoclay, there was an increase in the T_g of PSu to 184°C thus confirming strong interaction between hydroxyl group of the surfactant in C30B and PSu. The restriction imparted to the mobility of polymer chains as a result of intercalation of PSu chains within the silicate galleries might have led to the enhanced thermal stability. Similarly, PSu/C93A nanocomposite membranes also showed an increase in T_g to 183°C (Table III).

Proton conductivity

PEMs may need to exhibit optimum proton transport at high temperatures for better performance in

TABLE III
Differential Scanning Calorimetry

Sample	T_g onset (°C)	T_g midpoint (°C)
PSU	173	177
PSU/1% C30B	180	184
PSU/1% C93A	176	183

fuel cell applications. Proton conductivity of the membranes was calculated from resistance measurements within a temperature range of 30–60°C, and the result is depicted in Figure 5 and Table IV. The test was conducted at 100% RH, the most favorable condition for proton conduction as observed by Honma et al.[52] The conductivity measurement is crucial to assess the effect of various fillers.

Virgin PSu showed a wavy characteristics with a maximum conductivity at 40°C, which decreased with further increase in temperature up to 50°C and slightly increased at 60°C. This behavior indicates an unstable output which may affect the continuous power supply during service. All the membrane samples exhibited positive temperature–conductivity dependencies, suggesting an increase in conductivity at elevated temperature. Despite gradual increase in conductivity with temperature, the maximum conductivity of all the nanocomposites remained lower virgin PSu within the test range as evident from Figure 6. The decrease in proton conductivity with the addition of nanoclays may be attributed to the intercalated structure, which might have increased the proton transfer pathway, thus resulting in a lesser proton conductivity, as observed by Alberti and Casciola.[46]

Virgin PSu and PSu/C93A nanocomposite membranes showed similar conductivities at 30°C. With increase in temperature, PSu/C93A nanocomposites showed conductivity characteristics, which decreased at 40°C and increased thereafter. The decrease in conductivity of nanocomposite membrane shall be attributed to the presence of voluminous counter-ion without carboxylic acid attached to the nanoclay.[53] On the contrary, the incorporation of C30B had no appreciable effect on the conductivity, which is probably due to the poor contact between the electrolyte (membrane) and electrode despite an

TABLE IV
Conductivity of Virgin PSu and Nanocomposite Membranes at Different Temperatures

	Conductivity (10^{-7} S/cm) at different temperatures			
Sample	30 (°C)	40 (°C)	50 (°C)	60 (°C)
PSU	3.29 ± 0.56	3.82 ± 0.60	3.25 ± 0.59	3.51 ± 0.51
NaMMT	3.02 ± 0.77	3.12 ± 0.63	3.17 ± 0.68	3.33 ± 0.62
C93A	3.32 ± 0.41	3.24 ± 0.52	3.36 ± 0.54	3.41 ± 0.49
C30B	2.87 ± 0.53	2.93 ± 0.49	3.20 ± 0.61	3.31 ± 0.59

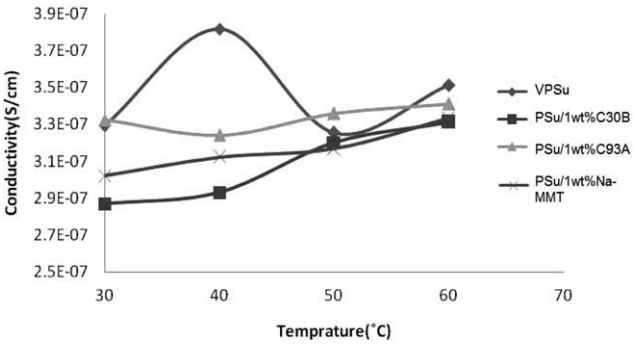

Figure 5 Conductivities of PSu and its nanocomposites.

increase in conductivity with temperature. Also, the presence of impermeable layered silicate sheets might have introduced tortuous pathways against penetrating molecules thus hindering the proton conduction. PSu/NaMMT nanocomposite membranes showed no appreciable increase in conductivity with temperature as observed by Thomassin et al.,[53] which may be due to the incompatibility of NaMMT with PSu. The longer diffusive route created as a result of dispersion of NaMMT might have hindered the proton transport. At elevated temperature (60°C), the conductivity of all membranes was comparable.

Single cell performance

Polarization curves for MEAs containing virgin PSu, PSu/1 wt % C30B, PSu/1 wt % C93A, and PSu/1 wt % NaMMT nanocomposite membranes were measured at 80°C to study their performance characteristics. The reactant gas pressures were maintained at 1.5 atm, and the flow rates of H_2 and O_2 at 200 mL/min and 400 mL/min, respectively. H_2/O_2 gases were humidified moderately prior to testing.

It is evident from the figure that the incorporation of organically modified nanoclays (C30B and C93A)

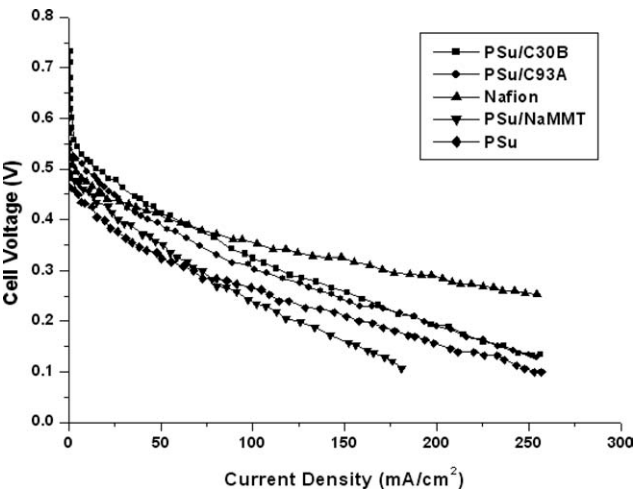

Figure 6 Polarization curves at 70°C.

increased the output voltage of virgin PSu membranes. Therefore, the polarization curves of PSu/1 wt % C30B and PSu/1 wt % C93A nanocomposite membranes are located above that of the virgin matrix and PSu/1 wt % NaMMT nanocomposite membranes. The output voltage of PSu/1 wt % NaMMT nanocomposite membranes was lesser than that of virgin PSu. This may be due to the incompatibility of the nanoclay with the matrix polymer. Furthermore, at 80°C, the humidification issue does not pose a dominant problem, because the membrane still has sufficient water for proton conduction.

However, the output of all the membranes was much lesser as compared with that of commercial Nafion membranes. Therefore, our forthcoming research will focus on studying the effect of sulfonation on the conductivity and cell performance characteristics of PSu.

CONCLUSIONS

PSu/layered silicate nanocomposite membranes were prepared using solvent casting technique. The membranes were prepared by solvent evaporation technique. NaMMT and organomodified clays were dispersed in the polymer matrix and their influence on the properties was investigated. Following conclusions were derived from the experimental findings.

- PSu/C30B nanocomposite membranes, prepared by solvent evaporation, showed optimum mechanical performance, and the corresponding membranes exhibited reduced water uptake characteristics. This may be attributed to the polar–polar interaction between C30B and PSu at the interface.
- The intercalation of PSu chains into clay galleries of C30B was confirmed from the increase in basal spacing from 18.5Å in C30B nanoclay to 24.3Å in the nanocomposite membranes.
- SEM micrographs revealed effective dispersion of nanoclays and improved pore distribution in PSu/C30B nanocomposite membrane. The distribution of pores in PSu/C30B is uniform as compared with other nanocomposite membranes.
- The incorporation of nanoparticles into the polymer matrix improved the thermal stability of the polymer and increased the T_g of PSu in the membrane.
- The conductivity studies revealed that PSu/1 wt % C93A nanocomposites showed better conductivity over the test temperature range that would favor undistributed power generation.
- The polarization curves obtained from single cell performance test showed the viability of PSu/clay nanocomposite membranes as proton exchange membranes in fuel cells.

The authors are thankful to Technology Systems Group, Department of Science and Technology for sponsoring the project.

References

1. Dhar, H. P. J Electroanal Chem 1993, 357, 237.
2. Appleby, A. J Philos Trans R Soc Lond A 1996, 354, 1681.
3. Shoesmith, J. P.; Collins, R. D.; Oakley, M. J.; Stevenson, D. K. J Power Source 1994, 49, 129.
4. Smitha, B.; Sridhar, S.; Khan, A. A. J Polym Sci B: Polym Phy 2005, 43, 1538.
5. Steck, A. E.; Stone, C. 2nd Int. Symp. on New Materials for Fuel Cell and Modern Battery Systems, Montreal, Canada, July 1997; p792.
6. Leung, L.; Bailly, C.; O'Gara, J. F.; Williams, D. J.; Karasz, F. E.; MacKnight, W. J Polym Commun 1987, 28, 20.
7. Helmer-Metzmann, F.; Osan, F.; Schneller, A.; Ritter, H.; Ledjeff, K.; Nolte, R.; Thorwirth, R. Eur Pat Appl574,7911993; p 23.
8. Zaidi, S. M. J.; Mikhailenko, S. D.; Robertson, G. P.; Guiver, M. D.; Kaliaguine, S. J Membr Sci 2000, 173, 17.
9. Alberti, G.; Casciola, M.; Massinelli, L.; Bauer, B. J Membr Sci 2001, 185, 73.
10. Johnson, B. C.; Yilgor, I.; Tran, C.; Iqbal, M.; Wightman, J. P.; Lloyd, D. R.; McGrath, J. E. J Polym Sci A: Polym Chem 1984, 22, 721.
11. Nolte, R.; Ledjeff, K.; Bauer, M.; Mulhaupt, R. J Membr Sci 1993, 83, 211.
12. Wang, F.; Hickner, M.; Kim, Y. S.; Zawodzinski, T. A.; McGrath, J. E. J Membr Sci 2002, 197, 231.
13. Zawodzinski, T. A.; Springer, T. E.; Uribe, F.; Gottesfeld, S. Sol St Ion 1993, 60, 199.
14. Karlsson, L. E.; Jannasch, P. Electrochim Acta 2005, 50, 1939.
15. Lufrano, F.; Baglio, V.; Staiti, P.; Arico', A. S.; Antonucci, V. Desalination 2006, 199, 283.
16. Iojoin, C.; Marechal, M.; Chabert, F.; Sanchez, J. Y. Fuel Cells 2005, 5, 344.
17. Alberti, G.; Casciola M.; Palombari, R. J Membr Sci 2000, 172, 233.
18. Zanetti, M.; Lonakin, S.; Camino, G. Macromol Mater Eng 2001, 279, 1.
19. Jung, D. H.; Cho, S. Y.; Peck, D. H.; Skin, D. R.; Kim, J. S. J Power Source 2003, 118, 205.
20. Genova-Dimitrova, P.; Baradie, B.; Foscallo, D.; Poinsignon, C.; Sanchez, J. Y. J Membr Sci 2001, 185, 59.
21. Jones, D. J.; Rozière, J. J Membr Sci 2001, 185, 41.
22. Boom, J. P.; Pünt, I. G. M.; Zwijnenberg, H.; de Boer, R.; Bargeman, D.; Smolders, C. A.; Strathmann, H. J Membr Sci 1998, 138, 237.
23. Vankelecom, I. F. J.; DeBeukelaer, S.; Uytterhoeven, J. B. J Phys Chem B 1997, 101, 5186.
24. Bottino, A.; Capannelli, G.; D'Asti, V.; Piaggio, P. Sep Purif Technol 2001, 22, 269.
25. Cornelius, C. J.; Marand, E. J Membr Sci 2002, 202, 97.
26. Aets, P.; van Hoof, E.; Leysen, R.; Vankelecom, I. F. J.; Jacobs, P. A. J Membr Sci 2000, 176, 63.
27. Merkel, T. C.; Freeman, B. D.; Spontak, R. J.; He, Z.; Pinnau, I.; Meakin, P.; Hill, A. J Chem Mater 2003, 15, 109.
28. Kreuer, K. D.; Weppner, W.; Rabenau, A. Angew Chem Int Ed Engl 1982, 21, 208.
29. Kreuer, K. D. J Membr Sci 2001, 185, 29.
30. Giannelis, E. P. Adv Mater 1996, 8, 29.

31. Choi, H. J.; Kim, S. G.; Hyun, Y. H.; Jhon, M. S. Macromol Rapid Commun 2001, 22, 320.
32. Riva, A.; Zanetti, M.; Braglia, M.; Camino, G. Polym Degrad Stab 2002, 77, 299.
33. LeBaron, P. C.; Wang, Z.; Pinnavaia, T. J. Appl Clay Sci 1999, 15, 11.
34. Vaia, R. A.; Price, G.; Ruth, P. N.; Nguyen, H. T.; Lichtenhan, J. Appl Clay Sci 1999, 15, 67.
35. Choi, Y. S.; Choi, M. H.; Wang, K. H.; Kim, S. O.; Kim, Y. K.; Chung, I. J Macromol 2001, 34, 8978.
36. Fischer, H. R.; Gielgens, L. H.; Koster, T. P. Acta Polym 1999, 50, 122.
37. Bharadwaj, R. K. Macromolecules 2001, 34, 9189.
38. Messersmith, P. B.; Giannelis, E. P. J Polym Sci 1995, A33, 1047.
39. Yano, K.; Usuki, A.; Okada, A.; Kurauchi, T.; Kamigaito, O. J Polym Sci 1993, A31, 2493.
40. Yano, K.; Usuki, A.; Okada, A. J Polym Sci 1997, A35, 2289.
41. Xie, W.; Gao, Z.; Pan, W. P.; Hunter, D.; Singh, A.; Vaia, R. Chem Mater 2001, 13, 2979.
42. Gilman, J. W. Appl Clay Sci 1999, 15, 31.
43. Silva, R. F.; Passerini, S.; Pozio, A. Electrochim Acta 2005, 50, 2639.
44. Chang, J. H.; Park, J. H.; Park, G. G.; Kim, C. S.; Park, O. O. J Power Source 2003, 124, 18.
45. Ruffmann, B.; Silva, H.; Schulte, B.; Nunes, S. P. Sol St Ion 2003, 269, 162.
46. Alberti, G.; Casciola, M. Annu Rev Mater Res 2003, 33, 129.
47. Herring, A. M. J Macromol Sci C: Polym Rev 2006, 46, 245.
48. Monticelli, O.; Bottino, A.; Scandale, I.; Capannelli, G.; Russo, S. J Appl Polym Sci 2007, 103, 3637.
49. Prasantha, K.; Park, S. G. J Appl Polym Sci 2005, 98, 1875.
50. Luo, M. L.; Zhao, J. Q.; Tang, W.; Pu, C. S. Appl Surf Sci 2005, 249, 76.
51. Jang, B. N.; Walkie, C. A. Polym 2005, 46, 9702.
52. Honma, I.; Nomura, S.; Nakajima, H. J Membr Sci 2001, 185, 83.
53. Thomassin, J. M.; Pagnoulle, C.; Caldarella, G.; Germain, A.; Jérôme, R. Polymer 2005, 46, 11389.